Cyclic plastic behavior of unidirectional SiC fibre-reinforced copper composites under uniaxial loads: An experimental and computational study

Stefan Kimmig[1] and Jeong-Ha You[*]

Max-Planck-Institut für Plasmaphysik, Boltzmannstr.2, 85748 Garching, Germany

[*]Corresponding author: Jeong-Ha You (you@ipp.mpg.de)

phone: ++49 89 3299 1373

fax: ++49 89 3299 1212

[1]: currently at MTU Aero Engines, Munich

Keywords

Copper matrix composites; Fiber-reinforced composites; SiC fibers; Heat sink materials; Cyclic plasticity; Cyclic tests; Mean field homogenization.

Abstract

Silicon carbide continuous fiber-reinforced copper matrix composites (Cu/SiC_f) offer huge potential as heat sink material for high-heat-flux applications at elevated temperatures (>300 °C) owing to the beneficial combination of strong, stiff and refractory SiC fibers with a highly conductive and ductile copper matrix. As high-heat-flux components are normally subjected to large temperature fluctuations combined with thermal strain variations, degradation of the Cu/SiC_f composites caused by fatigue damages under cyclic loads may affect the structural integrity of the component. In this study, the robustness of the Cu/SiC_f composites under cyclic loads at different temperatures was evaluated by means of uniaxial cyclic loading tests. The stability of the cyclic deformation hysteresis curves was used as a measure of material's durability. The experimentally observed global deformation behavior was interpreted with the help of a micromechanics-based theoretical model. It was shown that the Mori-Tanaka type mean field theory could describe the cyclic loading behavior of the composite quite well with a good fitting quality between the measured and simulated saturated cyclic curves. The effects of fiber content, applied strain range and test temperature are discussed.

1. Introduction

High-heat-flux (HHF) components are those machine parts which are subjected to severe thermal loads in various advanced technology sectors, e.g., nuclear fusion reactors, rocket propulsion or power electronics. HHF components are often equipped with actively cooled heat sink to enhance the heat exhaust performance. Mechanical reliability (strength) and heat removal capability (conductivity) are the major requirements for heat sink materials.

Conventionally, high-hardness copper alloys (e.g. precipitation hardened CuCrZr alloy, oxide particle-dispersed Cu) have been widely used as heat sink materials owing to their excellent conductivity and reasonably high strength and ductility [1-3]. But, copper-base materials can experience detrimental effects like softening and creep after long-term thermal exposure or by neutron irradiation at an elevated temperature (>300°C) [4, 5]. Such irreversible degradation occurs due to microstructural aging (e.g. Ostwald ripening of precipitates) or cascade damage (destruction of precipitates). In order to enhance the high-temperature strength, advanced heat sink materials with improved thermal stability and mechanical reinforcement are desired [6].

Silicon carbide continuous fiber-reinforced copper matrix composites (Cu/SiC_f) offer huge potential as heat sink material for HHF applications at elevated temperatures (>300°C) owing to the beneficial combination of strong, stiff and refractory SiC fibers with highly conductive and ductile copper matrix [7-9]. In a previous experimental work by the authors using Sigma SM 1140^+ fibers, approximately a rule-of-mixture type trend of ultimate tensile strength and elastic stiffness was achieved for a wide range of fiber volume fractions (V_f) ranging from 10 to 40 % at room temperature (RT) and at 300°C in full extent of strengthening effect as the theory predicts indicating the high fabrication quality of the composites (see Fig. 1) [9].

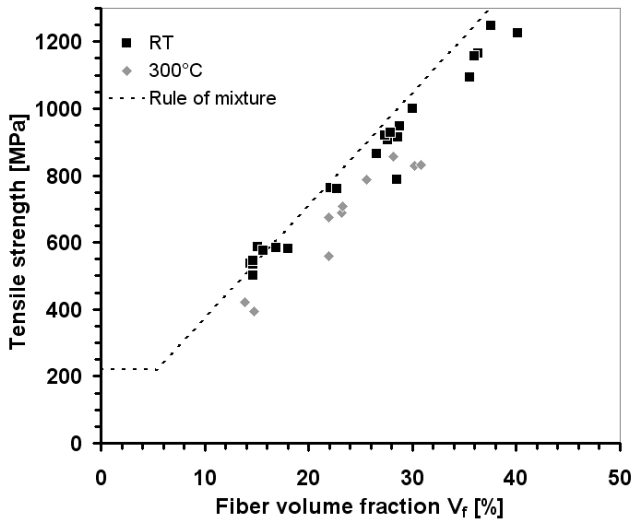

Fig. 1. Tensile strength data of Cu/SiC_f composite specimens reinforced with Sigma fibers measured at room temperature (black symbols) and 300°C (grey symbols) [9].

Moreover, Cu/SiC_f composites delivered excellent creep resistance (in fiber axial direction) at high temperatures (~650°C) [10].

HHF components are often subjected to a temporal variation of temperature gradients which may cause varying thermal stresses when thermal strains are fully or partly restrained. If the applied strain range is relatively large, the Cu/SiC_f composites will exhibit a low cycle fatigue (LCF) behavior owing to the ductile copper matrix which would undergo plastic yield. In this circumstance, the mechanical performance and durability of the composites under variable (or cyclic) loads at service temperatures will be significantly affected by the LCF damage. The impact of LCF on the microstructural integrity of continuous fiber-reinforced metal matrix composites can be categorized into two mechanisms, namely, matrix cracking leading to fiber fracture and loss of fiber bridging [11] and interfacial debonding and decreasing friction [12]. In literature most of the previous experimental testing studies of LCF for continuous fiber-reinforced metal matrix composites are focused on the fatigue crack growth behavior which was mostly investigated for continuous SiC fiber-reinforced titanium matrix composites [13, 14]. The data showed that the fatigue crack growth rate was considerably reduced compared to the unreinforced alloys. Dedicated LCF test studies conducted for fiber-reinforced copper matrix composites seem to be very scarce. There is a series of LCF testing works performed for tungsten monofilament-reinforced copper composite samples where the essential features of the cyclic hardening and the role of back stress due to filament-dislocation interaction were elucidated [15]. To author's knowledge, however, no previous work is found in the literature on the LCF performance or cyclic loading behavior of a Cu/SiC_f type composite.

In this paper, an experimental testing study on the cyclic loading behavior of unidirectional Cu/SiC_f composite specimens in the LCF regime is reported. A number of strain-controlled cyclic test data are presented for several different fiber volume fractions, applied strain ranges and test temperatures. In addition, the testing data are compared with the predictions of the theoretical simulation for interpreting the observed evolution of the cyclic stress-strain curves. The predictive capability of the theoretical model and the simulation tool is also discussed. The aim of this work is to investigate the cyclic plastic deformation behavior of the Cu/SiC_f composite (not to measure the LCF life) and to deliver original cyclic loading test data (e.g. saturated hysteresis curves) which can be utilized for calibrating the material parameters of the composites for cyclic plasticity modelling.

2. Experiment

2.1. Material fabrication

A commercial product of continuous SiC fiber (Sigma SM1140^{+}, diameter: 105µm) with carbon coating (3µm thick) was used for reinforcement. In order to strengthen interfacial bonding, the fibers were coated with a 200nm-thick titanium film as reactive agent by means of magnetron sputtering and further coated with a 500nm thick copper film to protect the Ti film from oxidation. Next, Cu mantle was deposited onto the pre-coated fibers to form matrix by means of electroplating in a $CuSO_4$ bath and the coated fibers were then heat-treated at 550°C (in vacuum) to form a stable TiC interfacial bonding layer and to out-gas hydrogen. Subsequently, the coated fibers were put into a cylindrical copper capsule with unidirectional array and consolidated by means of hot isostatic pressing under 100MPa at 650°C. A confocal laser microscope image of the unidirectionally reinforced Cu/SiC_f composite is shown in Fig. 2 (on the transversal cross section). The composite material was produced for two different fiber volume fractions (V_f = 15 and 29% for each). Finally, the hot-isostatic-pressed capsules were machined to produce cylindrical test specimens with mean diameter of 3.5mm and the gauge length of 14mm (Fig. 3). It is noted that the practical implementation of a cyclic testing was not straightforward for Cu/SiC_f composites due to the big difference in mechanical properties between the very soft matrix and the strong fibers. To ensure a uniform global straining of the gauge part without favored local deformation of the soft matrix, the dumbbell type specimen geometry was used to reduce the stress in the specimen grip zone. The clamping was realized by screws. The accuracy was not necessarily affected by shape, but probably by size. The length of the specimen was limited by the homogeneous heating volume of the inductive coil and the risk of buckling under compression.

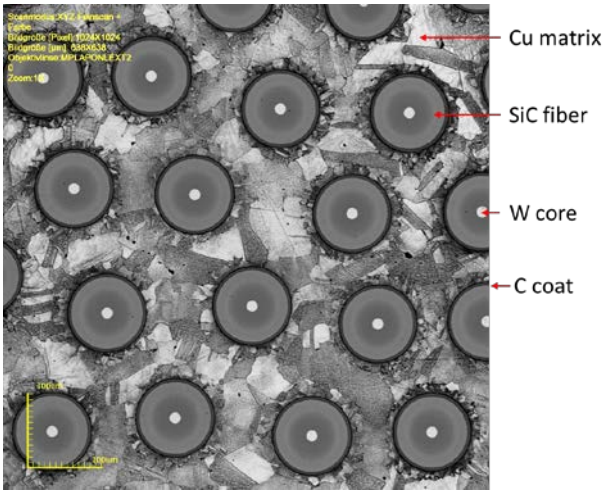

Fig. 2. A confocal laser microscope image of the unidirectionally reinforced Cu/SiC_f composite in the as-fabricated state (fiber diameter: 105µm).

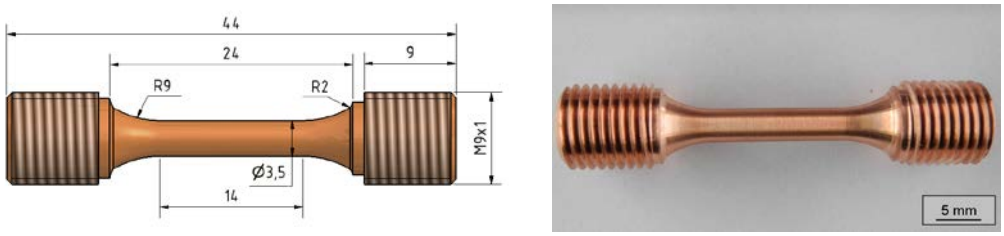

Fig. 3. Cu/SiC_f composite specimen used for cyclic test (dimension in mm).

2.2. Cyclic tests

Extensive cyclic tests were performed using a servo-hydraulic testing machine installed at MTU Aero Engines AG in Munich. The load cell had a maximum load capacity of 25kN and was calibrated according to the ASTM E4 class 1 prescription. The machine was equipped with an inductive heating coil (maximum possible heating rate: 20 C/s). In this experiment the applied heating rate was 3 C/s. The testing configuration was aligned according to the ASTM E1012 prescription. The testing was conducted in a strain-controlled mode where the strain measurement process was calibrated according to the ASTM E83 class B1 prescription (gauge length: 12mm).

Fig. 4 shows a composite specimen installed in the test rig with a strain gauge surrounded by the heating coil. A sawtooth-like triangular loading history consisting of tension, unloading and compression phases was repeatedly applied to the grip by the load cell at a constant strain rate of 0.001/s where viscous effect was assumed to be negligible. The tensile loading was limited up to a maximum elongation strain ranging between 0.25 - 0.55% while the reverse compressive loading was applied to null effective total strain. Compressive loads had to be applied to attain the original specimen length, since the copper matrix in the composite had already undergone plastic yield during tension. The fiber strains at the maximum elongation were far below the fracture strain of the SiC fiber (0.9%) so that the failure of embedded fibers in the composite specimens was very unlikely under the given test conditions. Test machine control parameters were adjusted according to the instruction of ASTM E 606 where the maximum error was kept below 1% of the applied strain range. The tests were conducted at RT and 300°C. The number of applied load cycles ranged from 100 to 1600 (300°C only). Testing at larger strain range was not pursued, since the specimen of the given geometry was still vulnerable to buckling under compression. Unfortunately, no statistical evaluation with multiple testing for each loading case was made due to a budgetary limitation.

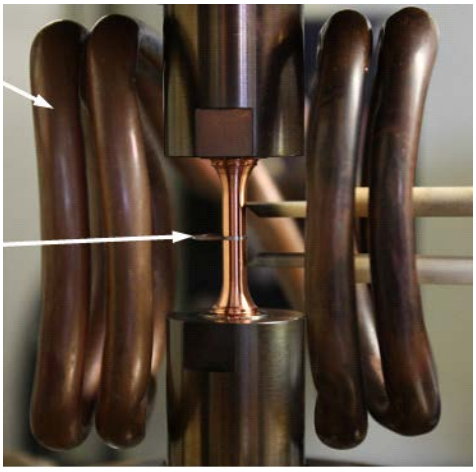

Fig. 4. Tensile test specimen of the Cu/SiC_f composite with unidirectional fiber reinforcement installed in a servo hydraulic test rig surrounded by an induction heating coil (gauge length: 12mm, diameter: 3.5mm). The specimen was equipped with a contact strain gauge and a thermocouple (indicated by an arrow).

3. Simulation

For the mechanical simulation of composite deformation under cyclic loading tests, a semi-analytical approach was applied which was based on the so called incremental Mori-Tanaka type mean field homogenization method, which is a nonlinear version of the originally elastic Mori-Tanaka theory so that plastic matrix can be modelled as well [16, 17]. This technique has already been applied for a dual scale finite element analysis of copper composite heat sink structures [18-20]. A detailed mathematical description of the model is given in Appendix. In this study, the simulation was conducted by means of a dedicated commercial code Digimat [21]. The code is capable of modelling the kinematic hardening of matrix under cyclic loads in addition to isotropic hardening.

In this work, combined nonlinear isotropic-kinematic constitutive law was assumed where the Frederick-Armstrong kinematic hardening model was applied [22]. The constitutive equations of the respective hardening components are given as follows [23]:

$$\sigma_e = \sigma_0 + Q \cdot \left[1 - e^{-b \cdot \varepsilon_{pl}}\right] \quad (1)$$

$$\dot{\alpha} = \frac{C}{\sigma_e}(\sigma - \alpha)\dot{\varepsilon}_{pl} - \gamma\alpha\dot{\varepsilon}_{pl} \quad (2)$$

where the meaning of the symbols is as follows.

σ_e: equivalent stress, σ_0: the initial size of the yield surface, Q: the maximum change in the size of the yield surface, b: the rate at which the size of the yield surface changes as plastic straining progresses, ε_{pl}: equivalent plastic strain, α: back-stress tensor, σ: stress tensor, C: the initial kinematic hardening modulus, γ: a constant determining the rate at which the

kinematic hardening modulus decreases with increasing plastic strains. The dot on the symbols denote rate. σ_o, Q, b, C and γ are temperature dependent material parameters to be calibrated. It was demonstrated in a previous study that the present constitutive model could capture the cyclic plasticity of copper and CuCrZr alloy very well for a wide temperature range [24].

The parameter calibration was carried out by means of multi-variable numerical regression in such a way that the simulated cyclic stress-strain curves were fitted to the measured test data for the evolution during the first 50 cycles, the saturated state and the convergence within the first 70 cycles. In Table 1, the elastic material properties of the SiC fiber (Sigma SM) and the Cu matrix are given. Computational simulation was carried out for different fiber volume fractions or test temperatures and compared with the experimental test data to evaluate the predictive capability of the micromechanics-based theoretical model. It should be noted that just because the plastic parameters of the matrix material is calibrated does not necessarily mean the global cyclic deformation behavior of the composite can be well reproduced in all features by the micromechanics model. The overall predictive capability of the computational tool essentially relies on the theoretical soundness of the underlying micromechanics model and numerical stability of the algorithm where the plastic parameters of the matrix play only a limited role.

Table 1. Elastic material properties of the SiC fiber (Sigma SM) and the Cu matrix

	Young's modulus	Poisson ratio	thermal expansion coefficient
SiC fiber	360GPa	0.17	5.7×10^{-6} K^{-1}
Copper	110GPa (RT) 90GPa (300°C)	0.34	16.6×10^{-6} K^{-1} (RT) 17.5×10^{-6} K^{-1} (300°C)

4. Results and discussion

4.1. Experimental tests

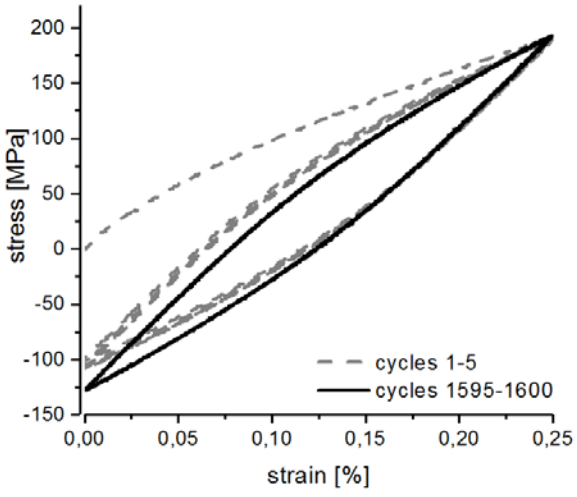

(a)

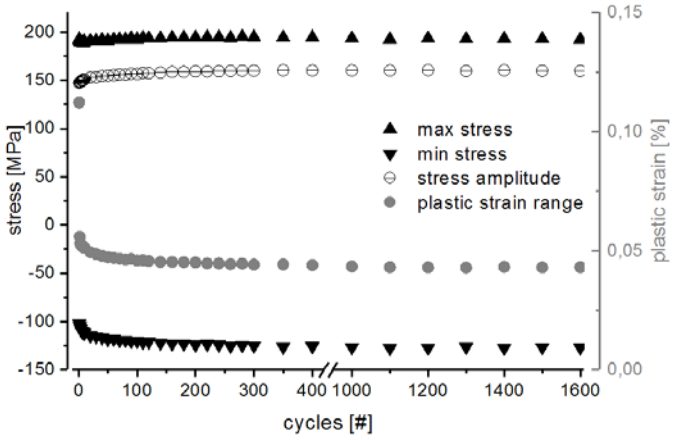

(b)

Fig. 5. Measured cyclic stress-strain curves (a) and the evolution of peak stress values under tension and compression together with the portion of plastic strain amplitude (b) of the Cu/SiC_f composite with V_f of 15% during the cyclic loading tests at RT ($\Delta\varepsilon$ = 0.25%).

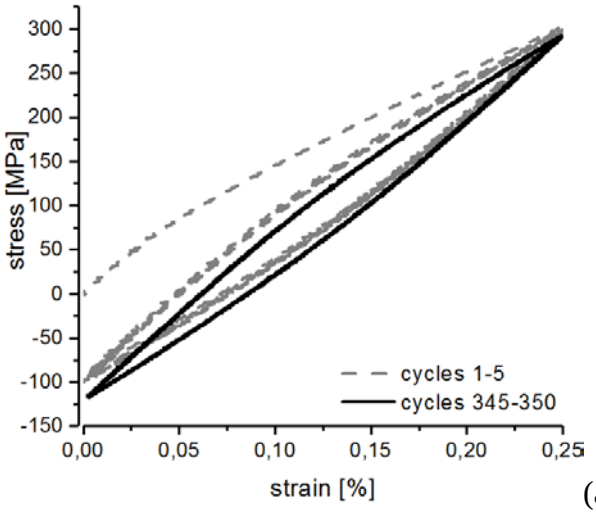

(a)

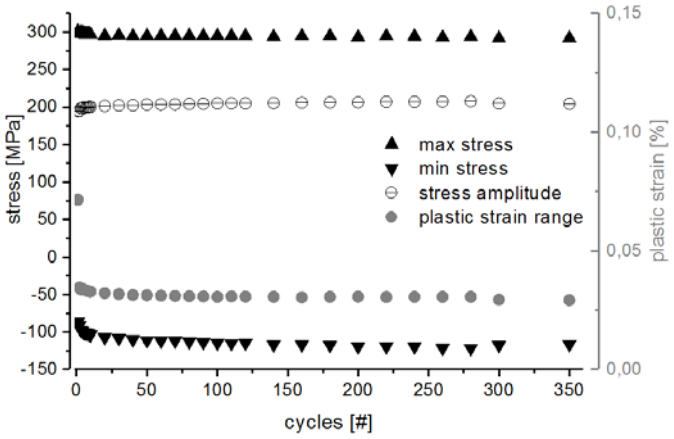

(b)

Fig. 6. Measured cyclic stress-strain curves (a) and the evolution of peak stress values under tension and compression together with the portion of plastic strain amplitude (b) of the Cu/SiC$_f$ composite with V_f of 29% during the cyclic loading tests at RT ($\Delta\varepsilon$ = 0.25%).

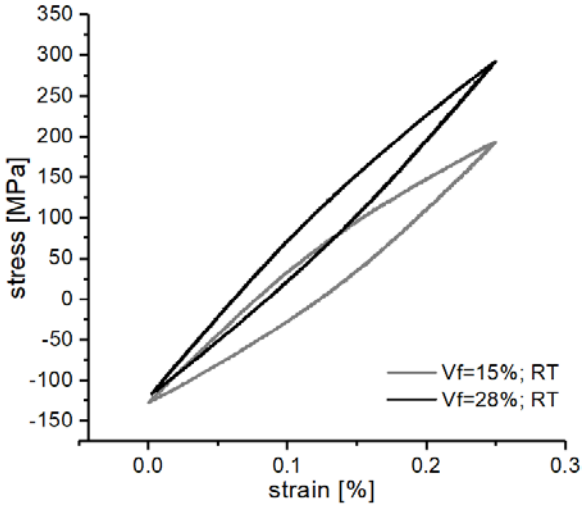

Fig. 7. Collated plots of the measured cyclic stress-strain curves (saturated curves only) of the Cu/SiCf composite during the cyclic loading tests at RT ($\Delta\varepsilon$ = 0.25%) for two different fiber volume fractions (V_f: 15% and 29%).

Fig. 5 (V_f = 15%) and 6 (V_f = 29%) show the measured cyclic stress-strain curves (a) and the evolution of the tensile and compressive peak stresses (b), respectively, together with the change in plastic strain range during the cyclic loading at RT. In Fig. 7, the final saturated hysteresis curves of Fig. 5(a) and Fig. 6(a) are collated in a single graph for direct comparison between the two test cases V_f = 15% and 29 % at RT ($\Delta\varepsilon$ = 0.25%). As described in section 2.2, all data plotted here were obtained for a specified total strain range respectively where loading and unloading was applied mostly in tensile regime. To highlight the change in cyclic deformation behavior, only the first five and the last five cycles are plotted for comparison.

The cyclic curves in Fig. 5 exhibit a remarkable nonlinear hysteresis behavior already in the early stage of loading indicating incremental inelastic dissipation, although the applied strain range was quite small (0.25% in total strain) [25]. The form of the hysteresis curves changed

only slightly during 1600 load cycles. As the fibers are elastic and the applied load was well below the fracture stress of the coated fiber (ca. 2.6GPa), the hysteresis could be attributed to the internal residual stress field produced by the plastic straining of the copper matrix. The role of internal residual stress fields of a fiber-reinforced metal matrix composite on the cyclic plastic dissipation feature (observed as a hysteresis) was clearly demonstrated in a unit cell-based computational study, where it was also shown that the presence of interfacial debonding even slightly reduced the area of hysteresis by relaxing the internal stress [26]. It was found in the fabrication study of the present Cu/SiC$_f$ composites that the fiber/matrix interface was mostly intact in the as-produced state exhibiting a good interfacial bonding quality [27]. The presence of any considerable initial flaws at interfaces was not observed in the microscopic inspection. After long-term thermal exposure (550°C, 400h), however, the Cu/SiC$_f$ composite specimens often showed damaged interface coatings (carbon layer) at several individual fibers where the affected interfaces were debonded or the fibers were cracked at much lower applied tensile stresses than the virgin ones [28].

Noting that the hysteresis loop formed already from the first loading cycle, the potential impact of any interfacial defects is deemed little relevant in the present testing case.

Indeed, the graph on the right shows that the plastic portion of the total strain range (0.25%) amounted ca. 0.04 - 0.05%. The cyclic curves stabilized within the first 200 load cycles where the plastic strain amplitude decreased asymptotically due to the strain hardening of the copper matrix. The magnitude of peak compressive stress increased slightly while the peak tensile stress remained nearly unaltered. No sign of fatigue deterioration was found.

The cyclic curves of the Cu/SiC$_f$ composite with the higher V_f (29%) exhibited higher peak tensile stress (ca. 300MPa) and a narrower width of the hysteresis which indicates a higher effective stiffness and reduced plastic dissipation. This response is consistent with the basic knowledge of composite micromechanics. The peak compressive stress was found to be nearly the same as in the case of V_f = 15%. The peak stresses in tension and compression entered into saturation already within 100 load cycles being much earlier than in the case of V_f = 15%. The very first tensile loading curves both in Fig. 5 and 6 deviated from the rest of the cyclic curves which formed loops. This feature seems to be a consequence of initial residual stress produced by the mismatch in the coefficient thermal expansion (CTE) between the matrix and the fibers in the fabrication process. It is well known that the yield surface of a Cu/SiC$_f$ composite is considerably affected in the presence of initial residual stress fields [29].

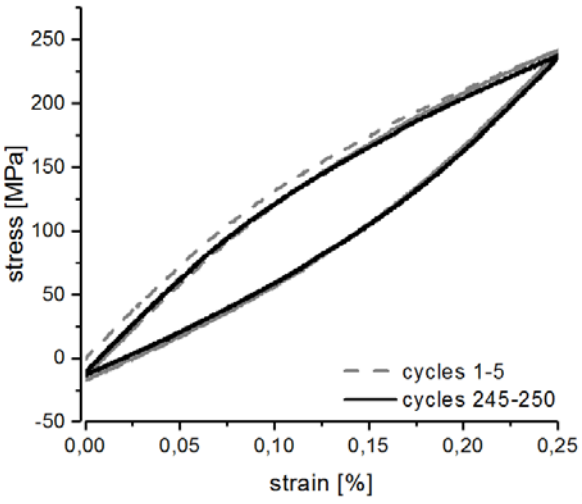

(a)

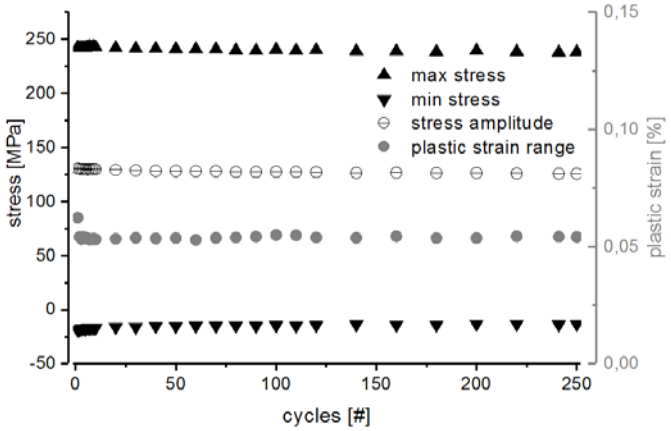

(b)

Fig. 8. Measured cyclic stress-strain curves (a) and the evolution of peak stress values under tension and compression together with the portion of plastic strain amplitude (b) of the Cu/SiC_f composite with V_f of 15% during the cyclic loading tests at 300°C ($\Delta\varepsilon$ = 0.25%).

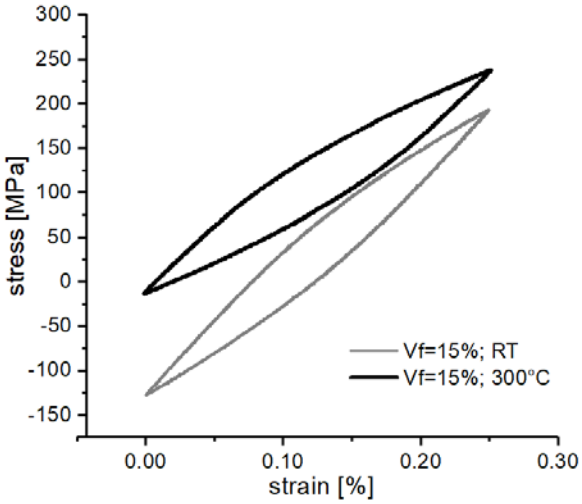

Fig. 9. Collated plots of the measured cyclic stress-strain curves (saturated curves only) of the Cu/SiC_f composite (V_f: 15%) during the cyclic loading tests ($\Delta\varepsilon$ = 0.25%) for two different testing temperatures (RT and 300°C)

Fig. 8 (V_f = 15%) shows the same kind of cyclic test data as in Fig. 5, but obtained at 300°C.

In Fig. 9 the final saturated hysteresis curves of Fig. 5(a) and Fig. 8(a) are collated in a single

graph for comparison between the test cases at RT and 300°C (V_f: 15 %, $\Delta\varepsilon$ = 0.25%). The cyclic curves at 300°C exhibit a premature saturation already from the first load cycle and remained fully stabilized during the following 250 load cycles. Moreover, the cyclic curves were shifted to the tensile direction and remained almost fully in the tensile stress regime. Consequently, a higher peak tensile stress (increase by approx. 50MPa) was attained while the null apparent elongation (zero total strain) was almost reached even by mere unloading (compressive stress of 20MPa). This situation roughly corresponds to a tensile loading-unloading test case. The magnitude of stress amplitude was slightly reduced. The immediate saturation of the cyclic curves together with the purely loading-unloading behavior indicates that the effect of initial residual stress field almost disappeared at 300°C. This indicates that the 'effective' stress-free temperature of the Cu/SiC_f composite may not have been higher than 300°C. The form and size of the hysteresis loops remained unchanged showing no cyclic strain hardening. This reveals the low yield stress and negligible contribution from the kinematic hardening of the matrix due to thermal softening. Nevertheless, the loading curves showed a relatively high work hardening rate owing to the efficient load transfer mechanism between the high-stiffness elastic fibers and the plastically deforming soft matrix [26].

An interesting behavior was the translational shift of the cyclic curves towards higher tensile stress regime in the uniaxial stress space departing from the compressive stress regime. It may be inferred that upon elastic unloading the effect of plastically induced internal residual stress field being partitioned between the fibers (tensile) and the matrix (compressive) might have been significantly relaxed by the reduced flow stress of the thermally softened matrix leading to a reduction of the apparent effective yield stress of the composite upon reversed loading. The thermally induced residual stresses produced by CTE mismatch are thought to have little effect on this shift, because such effect would readily vanish once the matrix had undergone overall plastic yield after first load cycles losing the memory of previous stress state. The global plastic hardening modulus was only slightly affected by the reduced flow stress of the matrix indicating that the plastic behavior was overwhelmed by the internal stress partition.

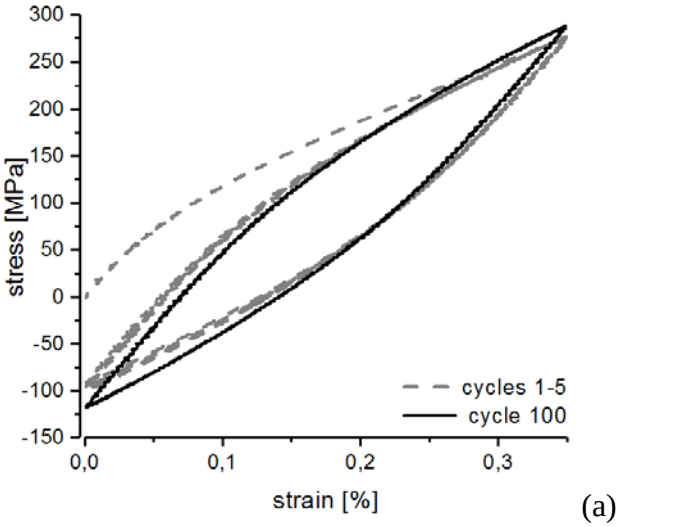

(a)

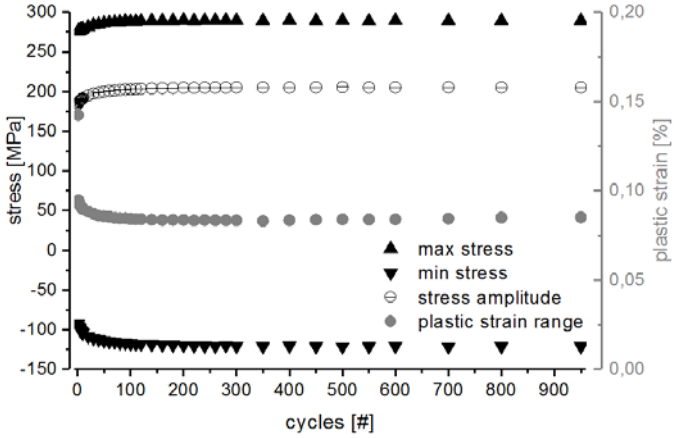

(b)

Fig. 10. Measured cyclic stress-strain curves (a) and the evolution of peak stress values under tension and compression together with the portion of plastic strain amplitude (b) of the Cu/SiC_f composite with V_f of 15% during the cyclic loading tests at RT ($\Delta\varepsilon$ = 0.35%).

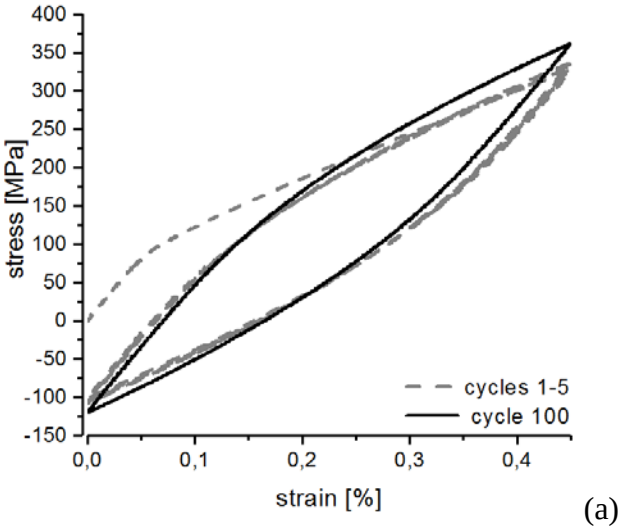

(a)

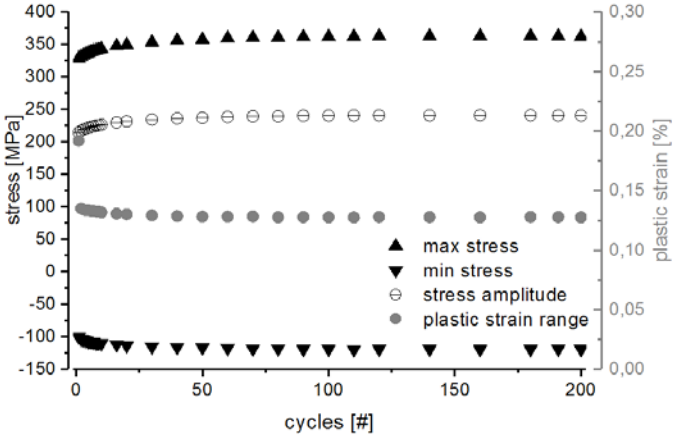

(b)

Fig. 11. Measured cyclic stress-strain curves (a) and the evolution of peak stress values under tension and compression together with the portion of plastic strain amplitude (b) of the Cu/SiC_f composite with V_f of 15% during the cyclic loading tests at RT ($\Delta\varepsilon$ = 0.45%).

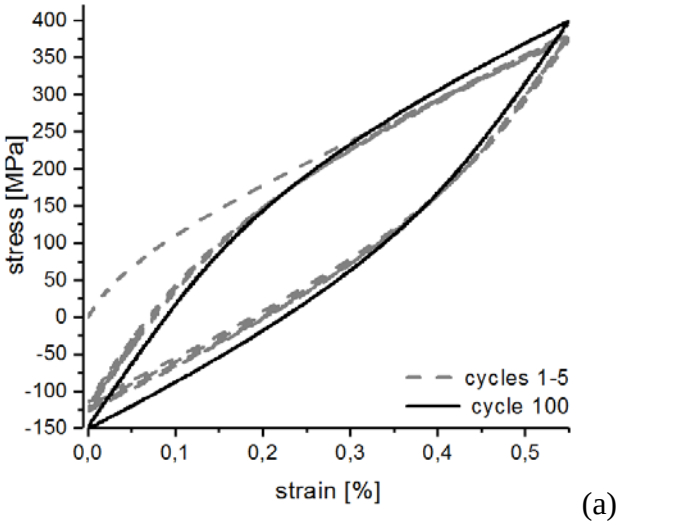

(a)

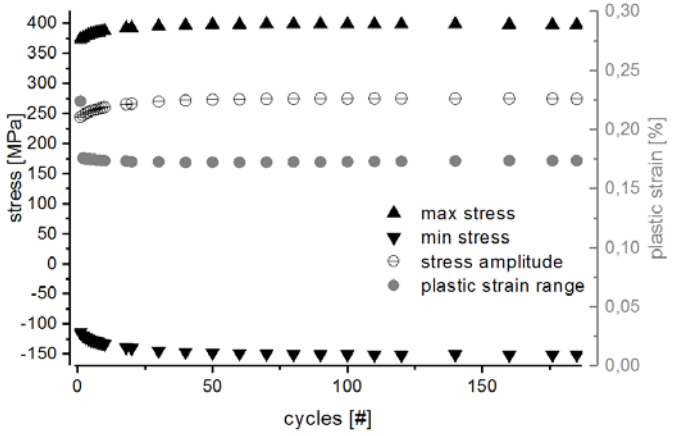

(b)

Fig. 12. Measured cyclic stress-strain curves (a) and the evolution of peak stress values under tension and compression together with the portion of plastic strain amplitude (b) of the Cu/SiC_f composite with V_f of 15% during the cyclic loading tests at RT ($\Delta\varepsilon$ = 0.55%).

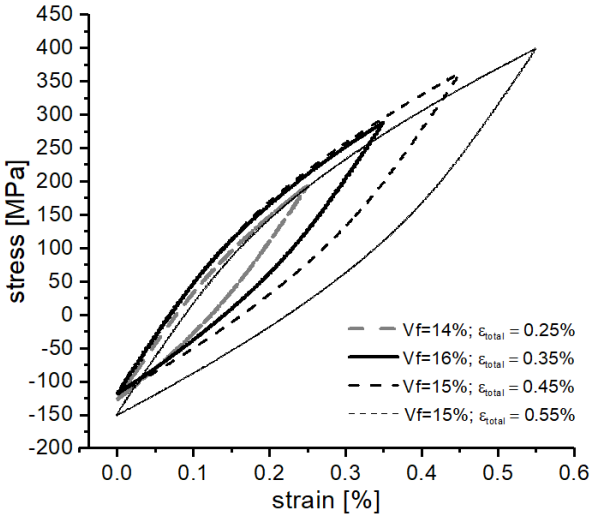

Fig. 13. Collated plots of the measured cyclic stress-strain curves (saturated curves only) of the Cu/SiC_f composite (V_f: 15%) during the cyclic loading tests at RT for different strain ranges.

Figs. 10-12 show the cyclic curves of the Cu/SiC_f composite with V_f = 15% tested at RT for three different applied strain ranges, namely, 0.35, 0.45 and 0.55%, respectively. In Fig. 13, the last saturated cyclic stress-strain curves of Figs. 5(a) and 10-12(a) are collated together in a single plot for comparing the effect of applied strain range at RT. The cyclic curves and the evolution of the peak stresses exhibit a qualitatively analogous saturation behavior as in Fig. 5 ($\Delta\varepsilon$ = 0.25%) whereas the width of the hysteresis loops and the peak stress values increased slightly with increasing strain range. A minor difference to the test case in Fig. 5 is that the peak tensile as well as peak compressive stresses increased slightly during the cyclic loading exhibiting a symmetric cyclic hardening in tension and compression. All the Cu/SiC_f composite specimens showed no sign of fatigue degradation up to at least 200 load cycles at the maximum strain range of 0.55% (950 cycles at $\Delta\varepsilon$ = 0.35%). in spite of the considerable amount of cyclic plastic dissipation (the area enclosed by the hysteresis loop).

The full history of cyclic peak stresses (maximum and minimum) exhibits an early saturation (Figs. 5(b), 6(b), 8(b), 10(b), 11(b), 12(b)) indicating a stable cyclic loading performance of the composite up to 1600 loading cycles without macroscopically discernable sign of progressive fatigue degradation for the given strain range and temperatures.

Another interesting feature is that the peak stresses in compression are the same at RT for different volume fractions (Fig. 7) and different strain ranges (Fig. 13) up to $\Delta\varepsilon$ = 0.45%. This indicates that fibres do not cooperate under compressive stress (or the contribution is negligible). In the case $\Delta\varepsilon$ = 0.55%, the compressive peak stress was slightly increased but the trend is roughly similar as that of the other loading cases. The cause of this slight increase is

unclear, probably might be due to stronger influence of neighboring fibers on the plastically induced residual stress field building in the matrix.

4.2. Simulation

Table 2. Plastic material parameters calibrated for the Cu/SiCf composite

	σ_o (MPa)	Q (MPa)	b	C (MPa)	γ
V_f=15 %, RT	44	40	150	100000	2500
V_f=29 %, RT	44	50	200	100000	1950
V_f=15 %, 300°C	35	10	0.1	66000	0.1

In Table 2, the plastic material parameters calibrated for the Cu/SiC_f composite are listed for three different test cases.

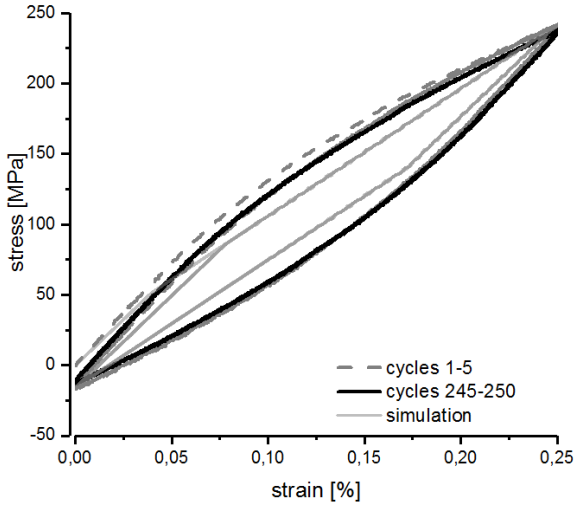

Fig. 14. Measured and theoretically simulated cyclic stress-strain behavior (1-70th cycles) of the unidirectional Cu/SiC_f composite under cyclic loads at 300 °C (V_f: 15%, $\Delta\varepsilon$ = 0.25%).

In Fig. 14, the theoretically simulated cyclic stress-strain behavior of the Cu/SiC_f composite at 300°C (V_f: 15%, $\Delta\varepsilon$: 0.25%, 1-70th cycles) are plotted and compared with the measured data (hysteresis loops for the 1-5th cycles and 245-250th cycles). It is found that the simulation underestimates the plastic effect as reflected by the narrower width of the hysteresis loop. On the other hand, the simulation accurately reproduced the effective elastic stiffness, the average plastic hardening modulus and the peak stresses. The simulated hysteresis loop looks like a polygon (parallelepiped) rather than a smooth curvilinear loop as the measured ones. This feature may be attributed to the mean-field homogenization on which the simulation is based. Here, the plastic yield criterion is assessed only considering field-averaged stress states in the matrix. In the framework of the mean-field homogenization, the onset of actual partial plastic yield in the region of local stress concentrations in the matrix (most likely near the fibers) is

suppressed due to rounded-off stress singularity. This artefact tends to produce a linearized stress-strain response even in a plastic deformation regime [27].

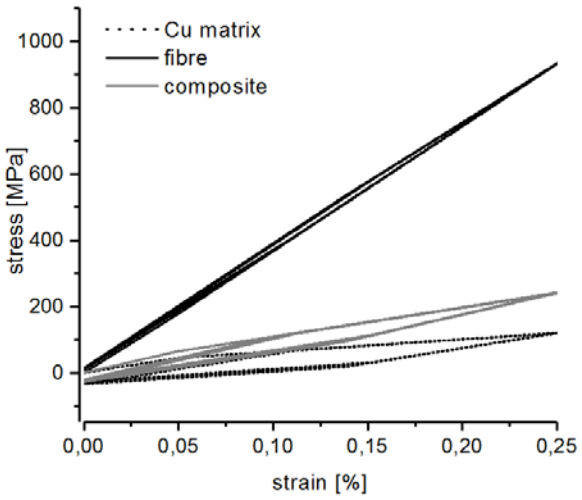

Fig. 15. Theoretically simulated cyclic stress-strain behavior of the reinforcing fiber and the matrix compared with those of the macroscopic Cu/SiC_f composite (V_f: 15%) under cyclic loads at 300°C.

In Fig. 15, the theoretically simulated cyclic stress-strain behavior of the reinforcing fiber and the matrix are plotted and compared with those of the macroscopic Cu/SiC_f composite (V_f: 15%) under cyclic loads at 300°C. The considered test condition is the same as in Fig. 14. The huge difference in the stress levels between the fiber and the matrix manifests the obvious effect of load partitioning between the constituents through the effective load transfer. In the present case, the stress partitioning was enhanced particularly by the high elastic modulus of the fiber and the low yield stress of the matrix. The resolved fiber stress reached ca. 900MPa at the total strain of 0.25%, and will reach 1800 MPa at 0.5%. Thus, the applied strain ranges in this study (up to 0.55%) could be regarded a safe loading regime excluding the risk of fiber fracture.

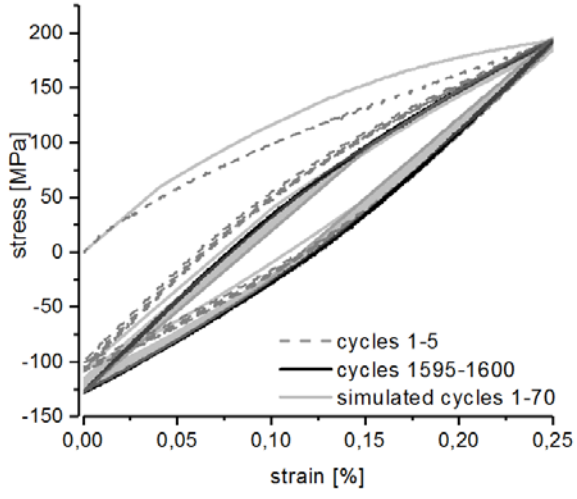

(a)

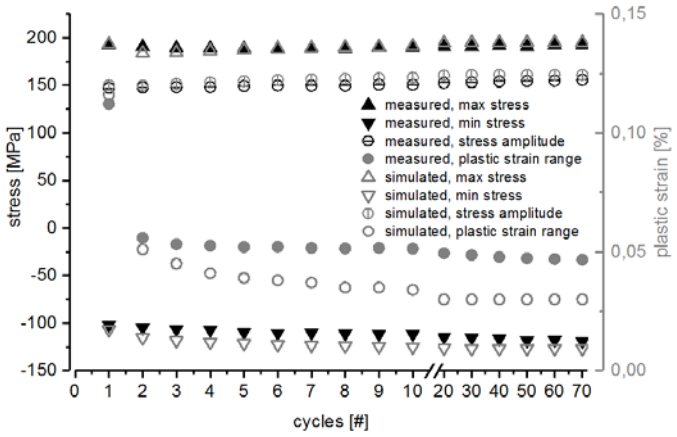

(b)

Fig. 16. Measured and simulated cyclic stress-strain curves (a) and the evolution of peak stress values under tension and compression together with the portion of plastic strain amplitude (b) of the Cu/SiC_f composite with V_f of 15% during the cyclic loading tests at RT ($\Delta\varepsilon$ = 0.25%).

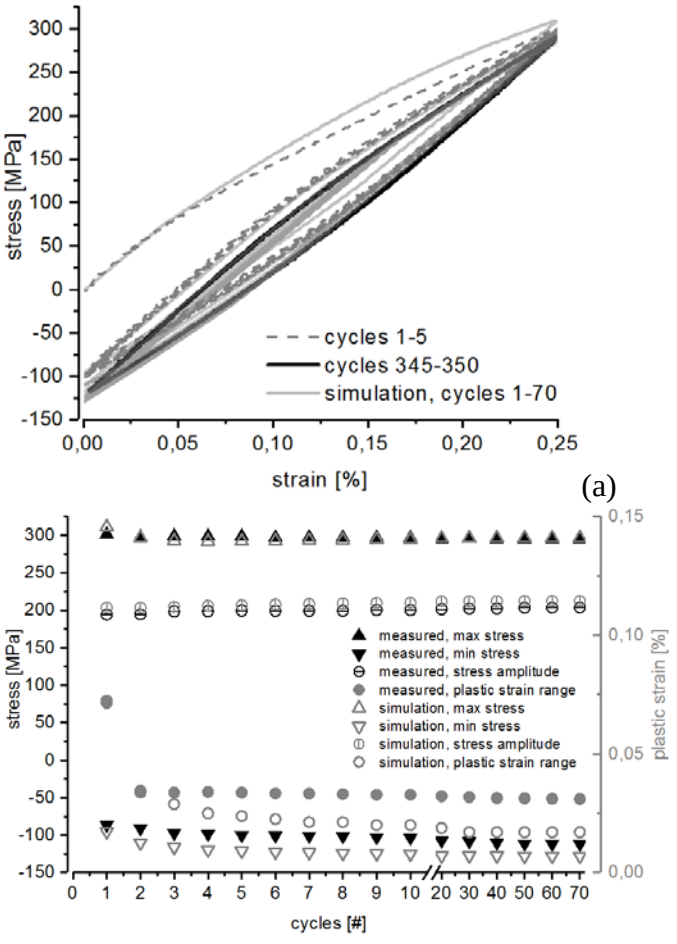

(a)

(b)

Fig. 17. Measured and simulated cyclic stress-strain curves (a) and the evolution of peak stress values under tension and compression together with the portion of plastic strain amplitude (b) of the Cu/SiC_f composite with V_f of 29% during the cyclic loading tests at RT ($\Delta\varepsilon$ = 0.25%).

In Fig. 16, the simulated cyclic stress-strain curves (left) of the Cu/SiC_f composite (V_f: 15%) at RT and the predicted peak stresses and plastic strain amplitude (right) are compared with the measured data, respectively. A similar comparison is given in Fig. 17 for the case of V_f = 29%. It is seen that the mean-field theory could reproduce the cyclic loading behavior quite well capturing the initial deformation feature as well as the transition to the stabilized state showing a good agreement in peak stress values with the measured ones for the whole period of cyclic loading. But, in the theoretical prediction, the plastic strain amplitude was notably underestimated due to the underestimated plastic dissipation (i.e. smaller hysteresis area) at both RT and 300°C (see Fig. 14). This limited modelling capability is thought to be a direct consequence of the mean-field approximation as mentioned above. Apart from this limitation, the modelling capability of the applied theoretical tool seems to be reasonable.

5. Summary and conclusions

In this study, the cyclic loading behavior and fatigue performance of unidirectional Cu/SiC_f composites were systematically investigated by means of extensive experimental cyclic tests and micromechanics-based theoretical simulations for two different fiber volume fractions (15% and 29%) each at RT and 300°C, respectively. The cyclic loads were applied in a strain-controlled mode where the total strain range was incrementally varied between 0.25% and 0.55%. For the tests, the composite material was fabricated and the specimens were produced in a laboratory scale. For the simulation, a dedicated commercial code was used which was based on the Mori-Tanaka type mean-field homogenization model with plastic formulation. The tensile test data showed a high level of reproducibility indicating high quality of material manufacture, specimen machining and testing process.

The major findings are summarized below:

1. The Cu/SiC_f composites underwent considerable plastic dissipation during individual load cycles even at the strain range of 0.25% as revealed in form of a hysteresis loop of saturated cyclic stress-strain curves.
2. The amount of incremental plastic work per each load cycle decreased at higher fiber volume fraction.
3. The measured cyclic curves exhibited rapid stabilization mostly within the first 50 - 100 load cycles.
4. At the elevated test temperature (300°C), the entire hysteresis loop was shifted to tensile stress regime escaping from the compressive stress, even though plastic yield took place. The effect of initial residual stress disappeared as well. It was inferred that

the relaxation of the plastically induced internal stresses due to the thermal softening of the matrix was the major cause of this.

5. The composites withstood at least up to 1600 loading cycles at RT and 250 cycles at 300°C without any signs of fatigue deterioration.
6. The theoretical simulation based on the mean-field homogenization well reproduced the stabilized cyclic stress-strain curves demonstrating the modelling capability for the composites even with a kinematic hardening feature under reversed loading.
7. The nonlinear mean-field theory combined with kinematic hardening model tended to underestimate the incremental plastic dissipation per load cycle.
8. Distinct stress partition due to load transfer was confirmed by the simulation.
9. The effect of test temperature and fiber content could be well captured by the applied theoretical model.
10. As only one test was made per each testing condition, the results are not complete and additional testing is required in order to confirm the findings presented here with a better statistics. In addition, the number of loading cycles needs to be increased up to ultimate fatigue rupture to investigate the fatigue damage evolution in the late stage of the fatigue life. Finally, the effect of applied strain range needs to be elucidated on the basis of more extensive experimental data.

Acknowledgement

The Authors would like to thank Dr. U. Siefken of Louis Renner GmbH in Dachau for the electron beam welding of the HIP capsules, K.-H. Süss of EADS in Ottobrunn for HIP and T. Brendel of MTU Aero Engines Munich for tensile tests. This work was partly carried out within the framework of the EUROfusion Consortium and has received funding from the Euratom research and training program 2014–2018 under grant agreement No 633053. The views expressed herein do not necessarily reflect those of the European Commission.

References

[1] Zinkle SJ. Applicability of copper alloys for DEMO high heat flux components. Phys Scr 2016;T167:014004 (10 pp).

[2] Riccius JR, Haidn OJ. Determination of linear and nonlinear parameters of combustion chamber wall materials. AIAA/ASME/SAE/ASEE Joint Propulsion Conference (AIAA 2003-4901), Huntsville, Alabama, 2003.

[3] You JH, Visca E, Bachmann Ch, et al. European DEMO divertor target: Operational requirements and material-design interface. Nucl Mater Energy 2016;9:171-176.
[4] Timmis W, Material assessment report on the use of copper alloys in DEMO. EFDA Report WP12-MAT02-M03 Copper alloys. 2013.
[5] Kalinin GM, Ivanov AD, Obushev AN, Rodchenkov BS, Rodin ME, Strebkov YS. Ageing effect on the properties of CuCrZr alloy used for the ITER HHF components. J Nucl Mater 2007;367-370:920-924.
[6] You JH. Copper matrix composites as heat sink materials for water-cooled divertor target. Nucl Mater Energy 2015;5:7-18.
[7] Brendel A, Paffenholz V, Köck Th, Bolt H. Mechanical properties of SiC long fibre reinforced copper. J Nucl Mater 2009;386–388:837–840.
[8] You JH, Bolt H. Overall mechanical properties of fiber reinforced metal matrix composites for fusion applications. J Nucl Mater 2002;305:14-20.
[9] Kimmig S, Allen I, You JH. Strength and conductivity of unidirectional copper composites reinforced by continuous SiC fibers. J Nucl Mater 2013;440:272-277.
[10] D. L. McDanels, Tungsten fiber reinforced copper matrix composites, NASA Technical Paper 2924, 1989.
[11] I. Greaves, J.R. Yates, The growth of freely initiating fatigue cracks in an unnotched SiC/titanium composite, Int. J. Fatigue 19 (1997) 151-159.
[12] D. P. Walls, F. W. Zok, Interfacial fatigue in a fiber-reinforced metal matrix composite, Acta Metall. Mater. 42 (1994) 2675-2681.
[13] P.J. Cotterill, P. Bowen, Fatigue crack growth in a fibre-reinforced titanium MMC at ambient and elevated temperatures, Composites 24 (1993) 214-221.
[14] S. A. Singerman, J. J. Jackson, Titanium metal matrix composites for aerospace applications, Superalloys 1996 (Ed. R. D. Kissinger et al.), The Minerals, Metals & Materials Society, 1996.
[15] J. Zhang, C. Laird, Cyclic hardening of tungsten-monofilament-reinforced monocrystalline copper matrix composites, Acta Mater. 47 (1999) 3811-3824.
[16] Tanaka K, Mori T. Average stress in matrix and average elastic energy of materials with misfitting inclusions. Acta Metall 1973;21(5):571-574.
[17] Pettermann HE, Plankensteiner AF, Böhm HJ, Rammerstorfer FG. A thermo-elasto-plastic constitutive law for inhomogeneous materials based on an incremental Mori–Tanaka approach. Comput Struc 1999;71(2):197-214.

[18] You JH. Triple scale failure estimation for a composite-reinforced structure based on integrated modeling approaches: Part l: Micro-scale analysis. Eng Fract Mech 2009;76:1425-1436.

[19] You JH. Design feasibility study of a divertor component reinforced with fibrous metal matrix composite laminate. J Nucl Mater 2005;336:97-109.

[20] You JH, Poznansky O, Bolt H. A comparative study on two elasto-plastic mean field methods. Mater Sci Eng A 2003;344:201-208.

[21] Digimat® 4.01 Documentation. e-Xstream Engineering. 2010.

[22] Armstrong PJ, Frederick CO. A mathematical representation of the multiaxial Bauschinger effect. C.E.G.B. Report RD/B/N 731. 1966.

[23] Chaboche JL. Constitutive equations for cyclic plasticity and cyclic viscoplasticity. Int J Plast 1989;5:247-302.

[24] You JH, Miskiewicz M. Material parameters of copper and CuCrZr alloy for cyclic plasticity at elevated temperatures. J Nucl Mater 2008;373:269-274.

[25] You JH, Kim BY, Miskiewicz M. Shakedown analysis of fibre-reinforced copper matrix composites by direct and incremental approaches. Mech Mater 2009;41:857–867.

[26] Ríos A, Martín-Meizoso A, You JH, et al. Micromechanical model of 3D cross-ply copper matrix composite reinforced with SiC fibres, Eng Failure Anal 2009;16:2559–2566.

[27] Kimmig, S Synthese und Charakterisierung von SiC-Faser-verstärktem Kupfer zur Anwendung in Hochleistungswärmesenken, Doctoral thesis, University of Würzburg, 2013.

[28] Kimmig S, Elgeti S, You JH. Impact of thermal exposure on a SiC fiber-reinforced copper composite. J Nucl Mater 2013;443:386–392.

[29] You JH, Bolt H. Prediction of plastic deformation of fiber-reinforced copper matrix composites. J Nucl Mater 2002;307-311:74-78.

Appendix. Mori-Tanaka type mean field constitutive model.

A1. Elastic formulation [11]

In this chapter, some fundamental relationships for the linear elastic case are shortly summarized. For elastic composite materials, the global (macroscopic) constitutive relation is written as:

$$\langle\sigma\rangle = E\langle\varepsilon\rangle, \text{ or } \langle\varepsilon\rangle = C\langle\sigma\rangle \quad \text{(A1)}$$

where E and C are the global elastic stiffness and compliance matrices, respectively. $\langle\ \rangle$ denotes the global volume averaged field quantities.

Similarly, the elastic constitutive relations for each phase p in micro-scale are written as:

$$\langle\sigma\rangle_{tot}^{(p)} = E^{(p)}\langle\varepsilon\rangle_{tot}^{(p)}, \text{ or } \langle\varepsilon\rangle_{tot}^{(p)} = C^{(p)}\langle\sigma\rangle_{tot}^{(p)} \quad \text{(A2-a, b)}$$

where $\langle\ \rangle_{tot}^{(p)}$ denotes the phase averaged total stress and strain state in the phase p. The superscript p can be either matrix m or fiber i, respectively.

A2. Incremental plastic formulation [12]

In the following, the incremental formulations of the Mori-Tanaka scheme and the corresponding algorithm to estimate the instantaneous state quantities for the elasto-plastic case are reviewed. The term 'rate' (denoted by d) is used for time derivatives whereas the term 'increment' (denoted by Δ) is employed for a sufficiently small finite increment in the framework of numerical integration algorithm.

The total averaged strain rates in micro-structural phase p can be related by far-field global averaged strain rate and instantaneous mean field strain concentration tensors:

$$d\langle\varepsilon\rangle_{tot}^{(p)} = \overline{A}_t^{(p)}\, d\langle\varepsilon\rangle_{mech} \quad \text{(A3)}$$

where the subscript t denotes instantaneous state and subscript *mech* mechanical contribution. $\overline{A}_t^{(p)}$ is the instantaneous mean field strain concentration tensor.

The global instantaneous tangent stiffness E_t can be written as:

$$E_t = E^{(i)} + (1-f)\left(E_t^{(m)} - E^{(i)}\right)\overline{A}_t^{(m)} \quad \text{(A4)}$$

where f is the volume fraction of fibers.

According to the Benveniste's formulation of the Mori-Tanaka mean field theory, the instantaneous mean field concentration tensors are written as,

$$\overline{A}_t^{(m)} = \left[(1-f)I + f\left[I + S_t C_t^{(m)}\left(E^{(i)} - E_t^{(m)}\right)\right]^{-1}\right]^{-1} \quad \text{(A5)}$$

in which the original elastic formulation is re-expressed in the instantaneous terms for each global strain increment. I denotes the fourth rank identity tensor and S_t represents the instantaneous Eshelby tensor which should be determined by numerical integration. Similar expressions exist for the instantaneous concentration tensors for the fiber.